

IMECE2010-37331

**CFD SIMULATION OF HUMAN COUGHS AND SNEEZES: A STUDY IN DROPLET
DISPERSION, HEAT, AND MASS TRANSFER**

Amir A. Aliabadi*

Department of Mechanical Engineering
University of British Columbia
Vancouver, British Columbia V6T 1Z3, Canada
Email: aliabadi@interchange.ubc.ca

Steven N. Rogak

Department of Mechanical Engineering
University of British Columbia
Vancouver, British Columbia V6T 1Z3, Canada
Email: rogak@mech.ubc.ca

Sheldon I. Green

Department of Mechanical Engineering
University of British Columbia
Vancouver, British Columbia V6T 1Z3, Canada
Email: green@mech.ubc.ca

Karen H. Bartlett

School of Environmental Health
University of British Columbia
Vancouver, British Columbia V6T 1Z3, Canada
Email: kbartlet@interchange.ubc.ca

ABSTRACT

A Computational Fluid Dynamics simulation of near-field cough and sneeze droplet dispersion and heat and mass transfer is developed. In this study various sources of variability in cough and sneeze processes are considered. These are variations in injection volume (0.5l, 2.5l, and 5.0l) and ambient relative humidity (20%, 40% and 60%). There are a total of 9 simulations for coughs and sneezes in a quiescent background. A large ensemble (5000) of droplets are tracked with diameters in the range 1-500micron. Evaporation and dispersion are predicted as a function of droplet size. Generally, fine droplets evaporate faster than large droplets. Higher relative humidities slow the evaporation process. Larger droplets have greater axial penetration. They also exhibit greater vertical drop due to the effect of gravity. Sideway penetration is increased by higher injection volumes. The buoyancy effect due to thermal energy of the injection is very weak, at least for the 10-second computation duration.

INTRODUCTION

Motivation

Recent outbreaks of Severe Acute Respiratory Syndrome (SARS) in 2002-2003 and the Swine Influenza in 2009 have

raised concerns about infection control worldwide. Airborne disease transmission involves generation, transformation, transport and finally inhalation of aerosols. Major sources of airborne pathogens are human forced expirations in the form of coughs and sneezes. Such forced expirations produce droplets that interact with ventilation airflow and transport infectious pathogens in buildings. Therefore, it is necessary to study the dispersion and heat and mass transfer of pathogen carrying expiratory droplets for better infection control strategies.

Our research focuses on ventilation design of healthcare facilities to reduce energy and airborne infection risk simultaneously. As a first step in predicting infection risk in a building, it is necessary to resolve spatial and temporal dispersion of aerosols in the ventilation domain. One approach is to decouple near-field (few meters) and far-field (whole ventilation space) dispersion processes since dispersion is governed by different physics at each level. For example, near-field physics include high turbulence, small time scales, weak buoyancy, and rapid heat and mass transfer between droplets and the background medium, while the converse is true for far-field. In this study we present the near-field dispersion of cough and sneeze droplets in a quiescent background using Computational Fluid Dynamics (CFD). In particu-

*Address all correspondence to this author.

lar, we study the dispersion, heat, and mass transfer of different size classes of droplets.

Literature on Cough and Sneeze Characterization

Various researchers have focused on droplet size of coughs and sneezes. Early studies in the field was initiated by microscopy measurements of droplets on filters and reported droplet sizes in the range 1-2000 μm with a peak of 8-16 μm for coughs and 4-8 μm for sneezes [1]. Using Optical Particle Counting (OPC), a later study indicated that most droplets are in the range 0.09-3.0 μm with the majority of droplets smaller than 0.3 μm [2]. OPC technique, however, is limited since it does not have a large radius detection range. In another study, the size distribution of droplets exhaled by healthy individuals was measured. It was found that in contrast to normal breathing, forced expirations produce larger droplets [3]. Other techniques such as Aerodynamic Particle Sizing (APS) and Scanning Mobility Particle Sizing (SMPS) were used to find the size distribution of droplets experimentally. A study found that total average size distribution of coughed droplet nuclei was in the range 0.58-5.42 μm and 82% of droplet nuclei centered at 0.74-2.12 μm . The entire average size distribution of the coughed droplets was in the range 0.62-15.9 μm and the average mode was 8.35 μm [4]. Another study considered characteristics of real coughs just after the mouth opening using Interferometric MIE Imaging (IMI). It was found that droplets were in the range 2-2000 μm with a mode of 4-8 μm [5]. However, accuracy of the IMI technique is limited to droplets only as small as 2-3 μm . Tab. 1 shows a summary of droplet size data in the literature.

TABLE 1. EXPERIMENTAL EXPIRATORY DROPLET SIZE

Study	$d_{min}[\mu\text{m}]$	$d_{max}[\mu\text{m}]$	$d_{mode}[\mu\text{m}]$
Cough [1]	1	2000	8-16
Sneeze [1]	1	2000	4-8
Cough [3]	<0.6	2.5	<0.6
Cough [4]	0.62	15.9	8.35
Cough [5]	2	2000	4-8
Cough [6]	1	>1471	1-2.9

Thermal characteristics of coughs and sneezes were investigated by some researchers. For example thermometry has been used to study nasal and oral exhalation temperatures as a function of environmental conditions such as ambient temperature and relative humidity [7]. Similarly, thermistor insertions in the respiratory tract provided thermal mapping of human airways as a function of environmental conditions and breathing rate. Only a small temperature range 33.9-35.5C for normal breathing was reported [8].

Flow characteristics of coughs and sneezes were also inves-

tigated in the literature. In a series of measurements a useful parameter in cough characterization has been defined as Cough Peak Flow Rate (CPFR) [9]. Previous research has shown that velocity-time profiles of coughs and sneezes are similar, but sneezes have higher peak velocities, and, in addition, there is some exhalation through the nose [10]. The peak flow rate in a cough may reach as high as 12L/s [11]. Particle Image Velocimetry (PIV) measurements and CFD simulations of cough droplet dispersion in a quiescent background found that the peak velocity varies in the range 6-22m/s and the average amounts of saliva injected are 6.1mg and 7.7mg for women and men respectively [12]. Another study has measured cough velocities of 11.7m/s on average [5]. The flow rate of coughs versus time for various subjects has also been measured. Another study related the Cough Peak Flow Rate (CPFR), Peak Velocity Time (PVT), and Cough Expired Volume (CEV) for various subjects [13].

The current literature lacks numerical studies with detailed prediction of size-resolved droplet dispersion and mass change. Most numerical studies assume droplets are small enough to behave like gases, Even studies that account for a discrete phase often ignore the evaporation process for simplification. These assumptions limit the model applicability to predict dispersion and mass change in real physical aerosol systems. This paper uses a multiphase model to account for droplet evaporation and dispersion behavior more accurately.

METHODOLOGY

Modeling Flow

Solving natural ventilation flow requires the integration and solution of mass, momentum, and energy equations. In the most concise way, conservation laws such as Navier-Stokes for mass, momentum and energy can be written in integral form as follows [14].

$$\frac{d}{dt} \int_{V(t)} Q dV + \oint_{S(t)} \mathbf{n} \cdot \mathbf{F} dS = \int_{V(t)} P dV \quad (1)$$

Modeling Droplet Heat and Mass Transfer

Multiphase modeling is suitable for droplet dispersion and heat and mass transfer in a continuum. In the discrete phase approach a large ensemble of droplets are injected in the continuum and equations of heat, mass, and motion are solved simultaneously. Neglecting radiation, the mechanisms for droplet mass and temperature change are convection and evaporation. Sherwood correlations relate mass transfer coefficient to the Reynolds and Schmidt numbers. In addition, they provide the Nusselt number, which relates the convective heat transfer coefficient to the Reynolds and Prandtl numbers [15, 16]. Having the time rate of change of droplet mass and the convective heat transfer coefficient, the energy balance equation for the droplet is derived as follows.

$$m_p c_p \frac{dT_p}{dt} = h A_p (T_\infty - T_p) + \frac{dm_p}{dt} h_{fg} \quad (2)$$

The trajectory of a discrete phase droplet can be determined by integrating the force balance written in the Lagrangian reference frame. This force balance equates the particle inertia with the forces acting on the droplet. The component form of this equation in the Cartesian coordinate can be written as follows.

$$\frac{d\vec{u}_p}{dt} = F_D(\vec{u} - \vec{u}_p) + \frac{\vec{g}(\rho_p - \rho)}{\rho_p} + \vec{F} \quad (3)$$

Modeling Turbulence

Cough and sneeze flows enforce high velocities of low viscosity gas through narrow openings, therefore, they are turbulent flows ($Re = \frac{\rho V d}{\mu}$). However, after the initial injection the turbulent energy declines due to mixing and viscous dissipation. As a result the Reynolds number decreases over time. The present study uses the Renormalization Group (RNG) $k - \epsilon$ turbulence model in Reynolds Averaged Navier-Stokes (RANS) simulations. Compared to the standard $k - \epsilon$ model, the RNG model has a better ability to model both high and low Reynolds numbers in the same flow. For these reasons various researchers have successfully implemented the RNG $k - \epsilon$ turbulence model for problems involving ventilation, air quality, and airborne infection risk in healthcare facilities [17–24].

Stochastic Droplet Tracking

In stochastic droplet tracking approach, we can predict the turbulent dispersion of droplets by integrating the trajectory equations for individual droplets by using the instantaneous fluid velocity along the droplet path during the integration. If we compute the trajectory for a large ensemble of droplets, then the random effect of turbulence has been accounted for. In the discrete Random Walk (DRW) model the fluctuating velocity components are discrete and piecewise constant functions of time. Their random value is kept constant over an interval of time given by the characteristic lifetime of the eddies [26].

In the DRW model, the interaction of a droplet with a succession of discrete fluid phase turbulent eddies is simulated. Each eddy is characterized by a Gaussian distributed random velocity fluctuation and a time scale. These fluctuating values can be sampled assuming they obey a Gaussian probability distribution with zero mean and unit variance. Since the kinetic energy of turbulence is known at each point and time in the flow, one can sample a fluctuating velocity assuming isotropy of turbulence. The droplet is assumed to interact with the fluid phase eddy over the smaller of the eddy lifetime and the eddy crossing time. When this time has reached, a new value of the instantaneous velocity is sampled and the calculation is repeated [26].

Two-way Coupling of Flow, Heat, and Mass Transfer

A realistic modeling of volatile droplet dispersion requires the consideration of heat, mass, and momentum exchanges between the discrete and continuous phases. For example, in real volatile droplet systems, droplets tend to evaporate hence losing heat to the continuous phase. Also the concentration of the

volatile species increases in the continuous phase by evaporation. In addition, the interaction of the droplet momentum by that of the continuous phase results in momentum exchange between the phases. A two-way coupling is accomplished by alternately solving the discrete and continuous phase equations until the solutions in both phases have converged within the required tolerances.

Space Discretization

Gambit 2.3.16 is used to generate the simulation grids. The simulation domain is a half box (due to vertical symmetry) 1m wide, 2m long, and 2m high. The expiration flow is initiated horizontally at the mid height through a round opening of 2cm² representing the mouth. There is also an exhaust outlet 0.2m high and 0.2m wide at the top of the face opposite to the injection. Three grids are generated with 76480, 114966, and 212888 control volumes respectively (coarse, mid, and fine levels). These grids have non-uniform mesh density. The mesh is refined near the injection area and at wall boundaries to resolve high shear flows more accurately at these locations. ‘‘Pave’’ face generation and ‘‘T-Grid’’ volume meshing algorithms are used to generate hybrid tetrahedral and hexahedral cells. Fig. 1 shows the computational domain. The momentum injection is on the x direction. The y axis shows the vertical direction and the z axis shows the sideways direction. Fig. 2 shows the mid level grid in the x-y plane.

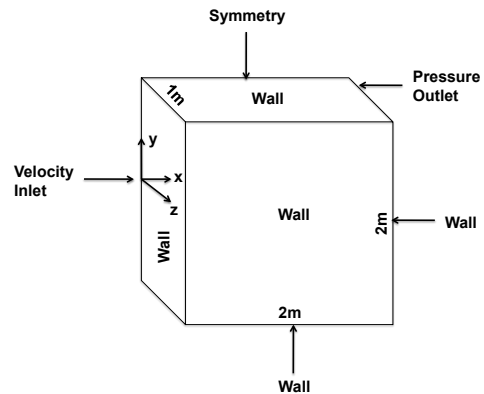


FIGURE 1. COMPUTATIONAL DOMAIN

Time Discretization

Of critical importance is the proper selection of the flow simulation and particle advancement time steps. For our cough and sneeze simulations time stepping is challenging. Part of the difficulty is that the correct selection of time step depends on many parameters such as, transient nature of flow, the space grid refinement, and the turbulent characteristics of the flow (eddy life time and length scale). Generally, the finer the temporal discretization for the continuous phase is, the more accurate the disper-

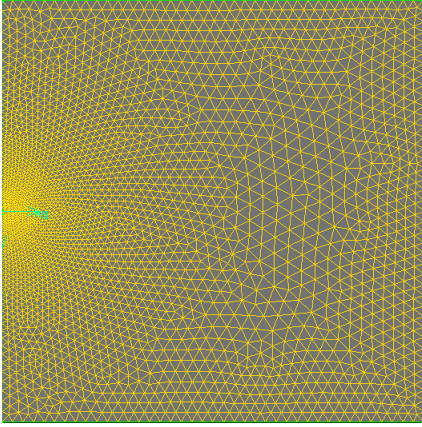


FIGURE 2. MID LEVEL GRID IN X-Y PLANE

sion calculation will be. The droplet tracking time step needs to meet three criteria. First, the tracking time step should be small enough to characterize the droplet motion only within the grid length scale. In other words, droplets should not cross more than one grid cell at each integration time step. Second, this time step must be smaller than that of the local eddy life time. Third, this time step must be smaller than the eddy crossing time. A non-uniform time step for the continuous phase is allowed with a resolution of 0.010s up to 1s and 0.100s up to 10s. The tracking time step for each fluid flow time step is 10 times finer with a further automated refinement option up to 100 times if necessary.

Boundary and Initial Conditions

For the cough and sneeze flows, careful implementation of boundary and initial conditions are required. The maximum amount of air that a human can expire relates to the Inspiratory Capacity (IC) and the Expiratory Reserve (ER) portions of human lung. IC is the maximum amount of air a person can inhale at the end of normal breathing cycle. ER is the maximum amount of air a person can exhale at the end of normal breathing cycle. The full lung contraction gives the maximum amount of air expiration from the lung. This is equal to sum of the IC and ER. The sum of IC and ER is on average 4.70L and 3.63L for men and women respectively. A normal cough would be only a fraction of this amount whereas a strong sneeze will be close to the full amount.

Experimental findings enables us to characterize the flow versus time profiles of human expirations [13]. A formulation has been developed to fit a mathematical model to an expiration given three parameters of Cough Peak Flow Rate (CPFR), Cough Expired Volume (CEV) and Peak Velocity Time (PVT). This formulation utilizes non-dimensionalizing flow rate and time and fits a double gamma distribution function to experimental data. There are also correlations between CEV and CPFR for both genders of men and women. The variation in PVT is in a limited

range and is insignificant compared to the total time of a cough or sneeze. Assuming a PVT of 0.1s and a value of CEV, one can fully describe a cough or sneeze flow versus time [13]. In such an approach the gender dependence of flow profile is insignificant.

Background temperature, expiration temperature, and humidity level are also sources of variability in the initial conditions. Since the variation in background temperature and expiration temperature in health care facilities is in a narrow range, we only consider the humidity level variation. The background temperature is assumed as 23C, the expiration temperature is assumed as 35C. The background fluid velocity is initialized to zero. The inlet is treated as velocity-inlet. The exhaust is treated as pressure-outlet. All the walls are treated as no-slip and adiabatic except for the symmetry face. The discrete phase is assumed to reflect at the boundaries.

An injection of a large ensemble of water droplets (5000) is considered. 94% of droplet volume fraction is assumed to be volatile. The remaining 6% has the same physical properties as water but does not evaporate. The nonvolatile volume fraction represents electrolytes, mucus, antibacterial compounds, and various enzymes in the actual saliva.

As discussed in the introduction, there is no unique droplet size distribution associated with coughs and sneezes. This is due to the inherent physiological variability in different subjects. Therefore, a distribution must be assumed that covers a wide range of droplet sizes with a representative mean. The Weibull distribution is used to bin injected droplets in the range 1-500 μ m. This distribution is also known as Rosin & Rammler since they were the first to apply it to describe the size distribution of particles. The probability density function for mass fraction of droplets is given as follows.

$$f(d, \bar{d}, n) = \frac{n}{\bar{d}} \left(\frac{d}{\bar{d}} \right)^{n-1} e^{-(d/\bar{d})^n} \quad (4)$$

The assumed distribution mean is 10 μ m and the spread constant is 0.1. Since the mass flow of fine droplets in coughs and sneezes is much greater than those of the large droplets, the logarithmic version of the Weibull distribution is used. In this version the same diameter range is converted to a range based on natural logarithm of the diameter ($\ln(d)$). Using this convention the mass flow in one bin would be less-heavily skewed as compared to the other bins. A particular choice of droplet size distribution does not affect the results of this study since the droplet concentration is so low that it does not influence the gas flow.

To present the size-classified results, the pre-evaporation mean diameter for each size bin is considered. The binning of data is performed in such a way to give more resolution at finer size droplets. For this purpose the 5000 droplets are grouped in 10 sizes that are binned successively for every 500 droplets. Tab. 2 shows the diameter range and the mean for the 10 size bins considered. In addition, the relaxation time τ and terminal velocity v_t are given for the mean diameter of each bin. The

relaxation time can be found using the particle size, mass, gas viscosity, and Cunningham correction factor [27]. In addition, calculation of the Reynolds number and the coefficient of drag gives the terminal velocity [27]. Independent of relative humidity, all droplets eventually evaporate to the nonvolatile core if they remain suspended in the air long enough.

TABLE 2. DROPLET DIAMETER RANGE, MEAN, RELAXATION TIME, AND TERMINAL VELOCITY FOR EACH BIN

Bin	$d_{min}[\mu m]$	$d_{max}[\mu m]$	$\bar{d}[\mu m]$	$\tau[s]$	$v_t[\frac{m}{s}]$
1	1.00	1.86	1.38	5.95e-6	5.84e-5
2	1.86	3.46	2.58	1.98e-6	1.94e-4
3	3.47	6.44	4.80	6.66e-5	6.53e-4
4	6.45	12.0	8.94	2.28e-4	0.0022
5	12.0	22.3	16.6	7.78e-4	0.0076
6	22.4	41.6	31.0	0.0027	0.0265
7	41.7	77.4	57.7	0.0093	0.0868
8	77.6	144	107	0.0321	0.2244
9	144	268	200	0.1119	0.6717
10	269	499	372	0.3871	1.4383

This ensemble of droplets is injected in the domain at the PVT of 0.1s with zero initial velocity. The droplets are staggered in the x direction over 0.01m. The selection of simulation cases are based on experimental findings. As noted in the methodology, CEVs of 0.5*l*, 2.5*l*, and 5.0*l* correspond to very weak, medium, and very strong human expirations. Also, the relative humidity in indoor conditioned air usually varies from 20% to 60%. As a result 9 simulation cases are chosen that represent these initial and boundary conditions (Tab. 3). The maximum injection velocity V_{max} at a distance of 0.1m from the mouth is also shown in Tab. 3. Note that these high velocities are instantaneous values and are expected to be higher than time averaged velocities reported in the literature.

TABLE 3. SIMULATION CASES [CEV: COUGH EQUIVALENT VOLUME, RH: RELATIVE HUMIDITY]

CEV [<i>l</i>]	$V_{max}[m/s]$	20% RH	40% RH	60% RH
0.5	1.5	1	4	7
2.5	42.0	2	5	8
5.0	89.9	3	6	9

CFD Solver

Fluent 6.3.26 is used to solve for the CFD simulation. In a coupled two-phase simulation, an iterative approach is taken to account for momentum, heat, and mass exchange between the two phases. For stochastic prediction of turbulent dispersion in the coupled two-phase flow calculations, we perform the stochastic dispersion each time the discrete phase trajectories are calculated during the coupled calculation.

For the continuous phase an implicit, pressure based solver with absolute velocity formulation is used. Green-Gauss cell based approach is chosen for the gradient option. A 2^{nd} order implicit time discretization is used. PREssure STaggered Option (PRESTO!) discretization is used for pressure. Contrary to standard pressure discretization, which interpolates pressures at the control volume faces, the PRESTO! scheme uses an alternate staggered mesh that stores pressure values at the faces. This way any interpolation or Neumann boundary condition assumptions are avoided. This is particularly helpful for buoyant flows where body forces are present and pressure gradient is not necessarily zero at all boundaries [28]. The Renormalization Group (RNG) $k - \epsilon$ turbulence model with differential viscosity and standard wall function is used. Viscous dissipation and buoyancy effects are also considered.

For the discrete phase, the trajectory equations, and for that matter any auxiliary equations describing heat or mass transfer to/from the droplet, are solved by stepwise direct integration over discrete time steps. We use a hybrid implicit and trapezoidal scheme to solve the discrete phase equations.

RESULTS AND DISCUSSION

Flow Solution

An earlier study validated the solver methodology for similar puff flows. Puff flows are a large class of flows that resemble coughs and sneezes and have been experimentally studied extensively. Puff flows can be characterized and validated using dimensionless axial and radial penetration versus time. Previous research shows that the dimensionless axial penetration should follow the $\frac{1}{4}$ law in the self preserved region [29, 30]. The dimensionless radial penetration should approach a constant value [31, 32]. Our earlier simulations conform with experimental puff penetration data.

Case 2 simulation is chosen to demonstrate droplet heat and mass transfer calculation and validation. A Grid Convergence Index (GCI) study confirmed that a velocity solution on the x -axis is reached within 5% of converged numerical value. The mid level grid is used for reporting the results.

Droplet Heat and Mass Transfer

Fig. 3 shows droplet diameter distribution at $t = 0.5s$. The binned diameters and temperatures for case 2 over the full simulation time ($t=10s$) are shown in Fig. 4 and 5. Droplet evaporation rate for water has an exact analytical solution [33]. For example, at 20% relative humidity and ambient conditions, the

evaporation times for $10\mu\text{m}$ and $100\mu\text{m}$ droplets to the non-volatile core are reported as 0.08s and 6.8s respectively [33]. The simulation predicts the evaporation for these droplets as $0.08 \pm 0.01\text{s}$ and $6.8 \pm 0.1\text{s}$ respectively. This validates the droplet heat and mass transfer model against the analytical solution. In general small droplets (bins 1 to 5) evaporate at much faster time scales (mili-seconds) than larger droplets (bins 6 to 10) for which the evaporation time is in the order of seconds.

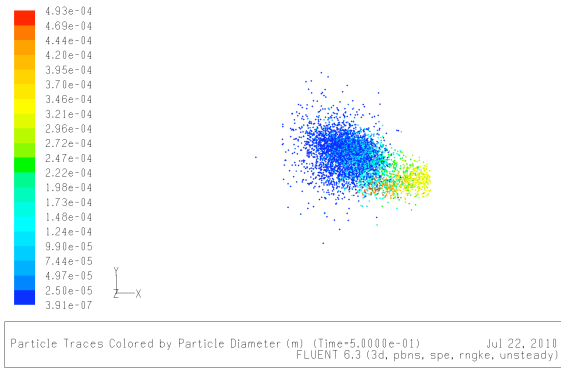


FIGURE 3. DROPLET DIAMETER (CASE 2)

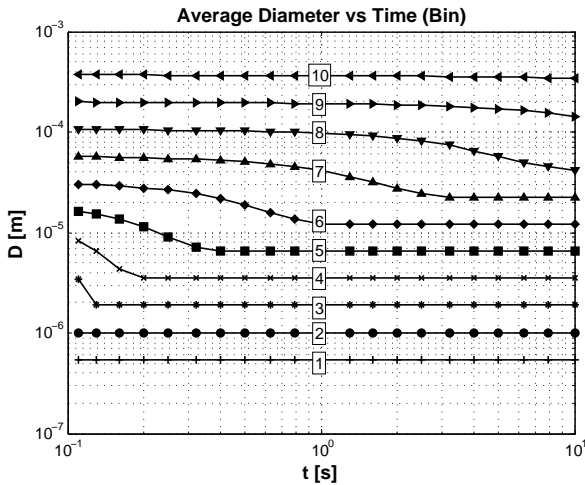


FIGURE 4. BINNED DROPLET DIAMETER CASE 2

Droplet Position

Average bin droplet positions can also be shown in the axial (x), vertical (y), and sideways (z) directions for case 2. Fig. 6, 7 and 8 show these respectively. For mean axial penetration, large size droplets (bins 8 to 10) penetrate fast initially since they have high momentum and the drag force reduces their speed slowly. In this case large droplets reach the opposite wall and reflect back

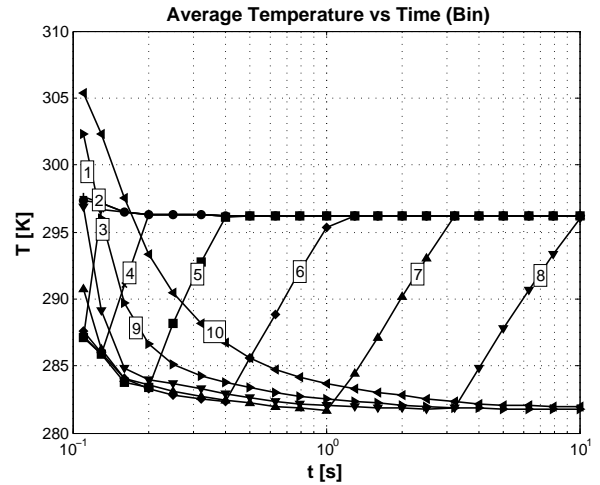


FIGURE 5. BINNED DROPLET TEMPERATURE CASE 2

into the domain. Small size droplets, on the other hand, are dispersed due to turbulent diffusion and move ahead rather slowly but steadily. For mean vertical penetration, large droplets (bins 7 to 10) are subject to gravity and drop to the bottom more quickly. On the other hand, small droplets are governed by turbulent diffusion and, on average, remain on the same vertical position. For mean sideways penetration small droplets (bins 1 to 8) diffuse more steadily due to turbulence while large droplets are concentrated close to the center.

The buoyant force due to thermal energy of a cough or sneeze is very weak, at least in the first 10 seconds, so that vertical displacement of fine droplets would only be pronounced if warm objects were present in the domain to drive a ventilation flow upwards.

Droplet Motion and Tracking Flow

An estimation can be made to determine what size droplets move along with the flow like fluid elements upon injection. For this purpose the Stokes diameter d_{Stk} can be calculated as a function of flow characteristic time. Any droplet smaller than d_{Stk} is expected to move like fluid elements. For an injected flow it is logical to choose the characteristic time as $\frac{D_{injection}}{V_{max}}$. d_{Stk} can be found using the following expression.

$$\frac{D_{injection}}{V_{max}} = \frac{V_{max} \rho_p \pi \frac{d_{Stk}^3}{6}}{F_{drag}(d_{Stk}, V_{max})} \quad (5)$$

Tab. 4 shows the estimated Stokes diameter for the shortest flow characteristic time (i.e. maximum velocity at PVT at a distance of 0.1m from the mouth) for the three CEVs in this simulation. For each case, all droplets with diameter smaller than that of Stokes are expected to move along with the flow upon injection.

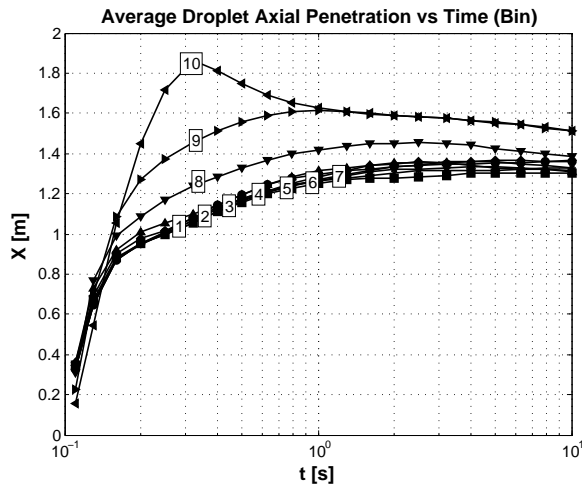


FIGURE 6. BINNED DROPLET AXIAL PENETRATION CASE 2

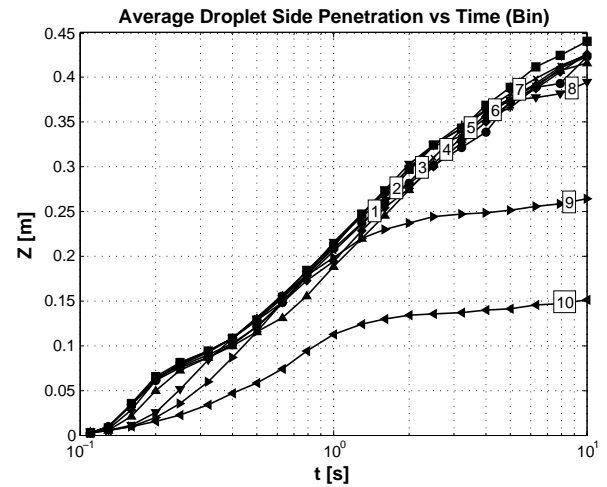


FIGURE 8. BINNED DROPLET SIDEWAY PENETRATION CASE 2

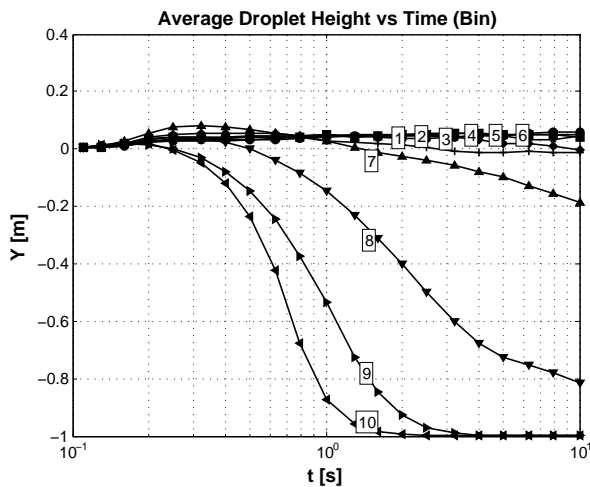


FIGURE 7. BINNED DROPLET VERTICAL PENETRATION CASE 2

TABLE 4. STOKES DIAMETER FOR DIFFERENT CEVS AT PVT

CEV[L]	V_{max} [m/s]	$\frac{D_{injection}}{V_{max}}$ [s]	d_{Stk} [μm]
0.5	1.5	1.07e-2	77.5
2.5	42.0	3.81e-4	38.1
5.0	89.9	1.78e-4	17.8

efficient, and hence the rate of evaporation, are reduced. The weak dependence of evaporation time on CEV can be explained using the concept of turbulent mixing. Water vapor concentration of the breath is near saturation and the less it mixes with the background air the more time is necessary to evaporate droplets. For example, the higher evaporation time for bin 7 in case 1 can be noticed.

Fig. 10 shows the axial penetration for different size bin droplets after 10s. The penetration of droplets is strongly affected by CEV so that in general higher CEVs result in higher axial penetration for all size bin droplets. A CEV of 0.5l can project droplet as far as 0.6m, whereas CEVs of 2.5l and 5.0l project droplets as far as 1.5m and 1.7m respectively. For CEV of 5.0l droplets in bins 9 and 10 reach the opposite wall and reflect back.

Fig. 11 shows the vertical penetration for different size bin droplets after 10s. The vertical penetration for all cases are similar, yet higher CEVs induce mixing in the domain so that, in general, longer time is needed to settle droplets. Within 10s, the vertical position of heavier droplets in bins 6 to 10 have been affected by gravity.

Fig. 12 shows the sideways penetration for different size bin

Effect of Cough Effective Volume and Relative Humidity on Droplet Evaporation and Dispersion

The 9 cough and sneeze simulations are run and the binned evaporation time, axial, vertical, and side penetration data are plotted. Fig. 9 shows the time of complete evaporation for different size bin droplets. Note that larger size bins of 8, 9, and 10 are not plotted since they do not evaporate fully within 10s. Evaporation time is strongly affected by relative humidity and weakly by CEV. In other words, these two mechanisms are decoupled. With higher relative humidities the water vapor concentration on the background medium is higher so that the mass transfer coef-

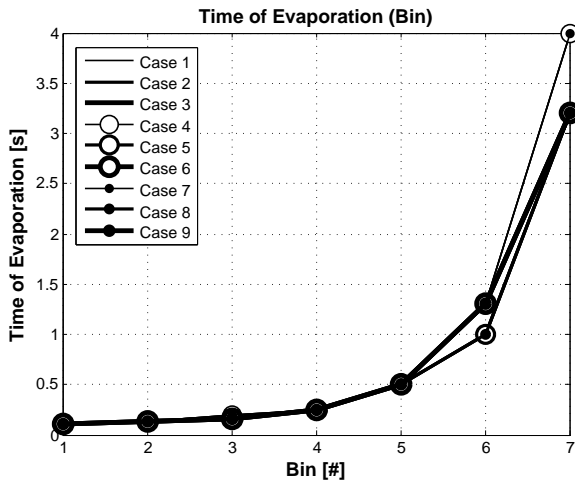


FIGURE 9. BINNED DROPLET EVAPORATION TIME

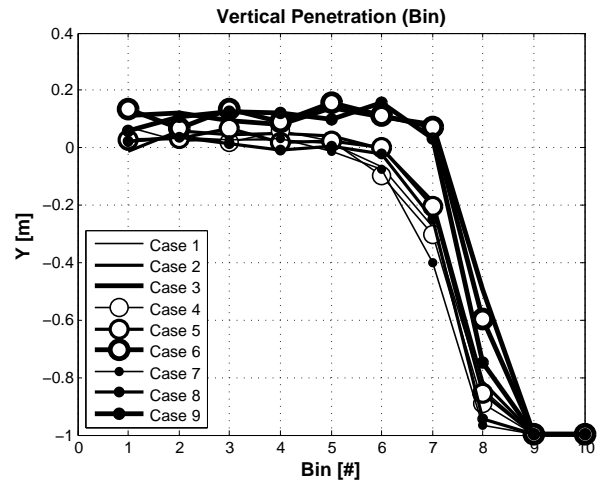


FIGURE 11. BINNED DROPLET VERTICAL PENETRATION

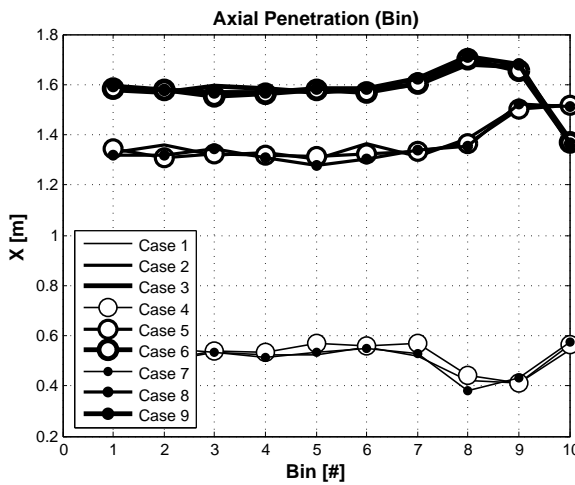


FIGURE 10. BINNED DROPLET AXIAL PENETRATION

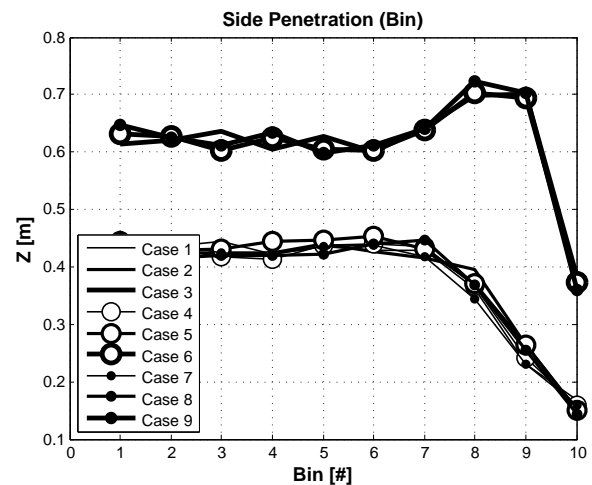


FIGURE 12. BINNED DROPLET SIDE PENETRATION

droplets after 10s. Again, side penetration is affected by CEV. The higher the initial injection volume, the higher turbulent mixing and therefore the higher dispersion in the z direction. It is noted that large droplets disperse less in the z direction since they have higher inertia and are not strongly subject to turbulent mixing. The sideways penetration can be as high as $0.7m$ for fine droplets injected with a CEV of $5.0l$.

Droplet Interaction With Ventilation Airflow Pattern

One design goal for any ventilation system is to remove the exhaled droplets by the airflow pattern. Particularly in ventilation design for healthcare facilities, this mechanism can reduce airborne infection risk. One such ventilation mechanism is dis-

placement ventilation that results in thermal stratification of air in a room.

The removal mechanism of droplets by thermal air stratification can be understood by comparing droplet terminal velocity and the bulk upward airflow velocity. In general, if the droplet terminal velocity is less than the bulk upward airflow velocity, the droplets can be transported to the ceiling and eventually removed through the exhaust.

Although the above approximation is useful, the actual removal of droplets by air stratification depends on details of the airflow pattern. In general the bulk upward motion of air in displacement ventilation is a crude model and not a representation

of reality. For example, a poorly designed displacement ventilation system can cause “downwash” airflow at non-adiabatic walls that can move droplets down. Also, the flow tends to go upwards only at specific sites where strong thermal plumes exist. Therefore, it is essential for droplets to be captured in the thermal plumes for effective removal. Otherwise, they may circulate for a long time in the room.

CONCLUSIONS

Predicting infection risk due to human generated airborne pathogens in healthcare facilities requires detailed knowledge of droplet generation and dispersion mechanisms. In this study, Computational Fluid Dynamics (CFD) is used to simulate near-field cough and sneeze droplet dispersion, heat, and mass transfer in a quiescent background.

It is found that droplet evaporation time strongly depends on the original size bin and relative humidity. Droplets evaporate to the non-volatile core more slowly at higher relative humidities. Axial penetration of droplets is strongly affected by injection volume. In general, larger size bin droplets have a higher initial momentum and travel the longest axial distance from the injection point. Vertical penetration results show that larger size bin droplets drop below the breathing zone due to gravity, while finer droplets remain closely at the original vertical position. The sideway penetration is higher for larger injection volumes due to turbulent mixing.

The evaporation model in this study is useful and provides physical time scales for heat and mass transfer between droplets and background air. This model validates against analytical solutions and can be used with both simplistic and time-space resolved dispersion models. To predict detailed droplet removal mechanisms in healthcare facilities, however, it is required to perform CFD analysis of droplet dispersion, heat, and mass transfer in case-specific ventilation systems.

ACKNOWLEDGMENT

Special thanks go to colleagues Peter Anderson, Mahdi Salehi, and Edward Chan whose expertise and guidelines in CFD modeling was very helpful towards the completion of this study. We also thank Natural Sciences and Engineering Research Council (NSERC) of Canada and Stantec for providing the funding for this project.

NOMENCLATURE

c_p Specific Droplet Heat Capacity, $J/kg - K$
 d Droplet Diameter, m
 \bar{d} Mean Droplet Diameter, m
 f Droplet Mass Fraction Probability Density Function, $1/m$
 \vec{g} Gravitational Acceleration, m/s^2
 h Convective Heat Transfer Coefficient, $J/m^2 - K$
 h_{fg} Latent Heat of Vaporization, J/kg
 k Turbulent Kinetic Energy, m^2/s^2
 m_p Droplet Mass, kg

n Spread Constant
 \mathbf{n} Unit Normal Vector to Surface
 r Uniform Random Number (0-1)
 t Time, s
 \vec{u} Continuous Phase Velocity, m/s
 \vec{u}_p Droplet Velocity, m/s
 v_t Droplet Terminal Velocity, m/s
 A_p Droplet Surface Area, m^2
 $D_{injection}$ Injection Diameter, m
 d_{Stk} Stokes Diameter, m
 \vec{F} Acceleration Per Unit Mass, m/s^2
 \mathbf{F} Tensor Containing Flux of Conserved Quantities
 F_D Drag Acceleration Per Unit Velocity, $1/s$
 F_{drag} Drag Force, N
 P Rate of Production of Conserved Quantities
 Q Vector of Conserved Quantities
 Re Reynolds Number
 $S(t)$ Surface Area as a Function of Time, m^2
 T Continuous Phase Temperature, K
 T_p Droplet Temperature, K
 T_∞ Far-Field Temperature, K
 V Volume, m^3
 $V(t)$ Volume as a Function of Time, m^3
 V_{max} Maximum Flow Velocity, m/s
 ε Turbulent Dissipation Rate, m^2/s^3
 ρ Continuous Phase Density, kg/m^3
 ρ_p Droplet Density, kg/m^3
 τ Droplet Relaxation Time, s
CEV Cough Equivalent Volume, m^3
CPFR Cough Peak Flow Rate, m^3/s
DNS Direct Numerical Solution
DRW Discrete Random Walk
ER Expiratory Reserve, m^3
GCI Grid Convergence Index
IC Inspiratory Capacity, m^3
LES Large Eddy Simulation
PVT Peak Velocity Time, s
RANS Reynolds Averaged Navier-Stokes
RNG Renormalization Group
RH Relative Humidity, %

REFERENCES

- [1] Duguid, J. P., 1946. “The size and duration of air carriage of respiratory droplets and droplet nuclei”. *Hyg.*, **44**, pp. 471–479.
- [2] Fairchild, C. I., and Stamper, J. F., 1987. “Particle concentration in exhaled breath”. *Am. Ind. Hyg. Assoc. J.*, **48**, pp. 948–949.
- [3] Papineni, R. S., and Rosenthal, F. S., 1997. “The size distribution of droplets in the exhaled breath of healthy human subjects”. *Journal of Aerosol Medicine*, **10**(2), pp. 105–116.

- [4] Yang, S., Lee, G. W. M., Chen, C.-M., Wu, C.-C., and Yu, K.-P., 2007. "The size and concentration of droplets generated by coughing in human subjects.(report)". *Journal of Aerosol Medicine*, **20**(4), 12/01, pp. 484–494.
- [5] Chao, C. Y. H., Wan, M. P., Morawska, L., Johnson, G. R., Ristovski, Z. D., Hargreaves, M., Mengersen, K., Corbett, S., Li, Y., Xie, X., and Katoshevski, D., 2009. "Characterization of expiration air jets and droplet size distributions immediately at the mouth opening". *Journal of Aerosol Science*, **40**(2), pp. 122–133.
- [6] Loudon, R. G., and Roberts, R. M., 1967. "Relation between the airborne diameters of respiratory droplets and the diameter of the stains left after recovery". *Nature*, **213**, pp. 95–96.
- [7] Höpfe, P., 1981. "Temperatures of expired air under varying climatic conditions". *Int. J. Biometeor*, **25**(2), pp. 127–132.
- [8] McFadden, E. R., Pichurko, B. M., and Bowman, H. F., 1985. "Thermal mapping of the airways in humans". *American Physiological Society*, **58**(2), pp. 564–570.
- [9] Piirila, P., and Sovijarvi, A. R. A., 1995. "Objective assessment of cough". *Eur. Respir. J.*, **8**, pp. 1949–1956.
- [10] Nishino, T., 2000. "Physiological and pathophysiological implications of upper airway reflexes in humans". *Japanese Journal of Physiology*, **50**, pp. 3–14.
- [11] McCool, F. D., 2006. "Global physiology and pathophysiology of cough: Accp evidence-based clinical practice guidelines". *American College of Chest Physicians*, **129**, pp. 48S–53S.
- [12] Zhu, S., Kato, S., and Yang, J.-H., 2006. "Study on transport characteristics of saliva droplets produced by coughing in a calm indoor environment". *Building and Environment*, **41**(12), pp. 1691–1702.
- [13] Gupta, J. K., Lin, C. H., and Chen, Q., 2009. "Flow dynamics and characterization of a cough". *Indoor Air*, **19**, pp. 517–525.
- [14] Lomax, H., Pulliam, T. H., and Zingg, D. W., 2001. *Fundamentals of Computational Fluid Dynamics*. Springer-Verlag Berlin Heidelberg, Germany.
- [15] Ranz, W. E., and Marshall, W. R., 1952. "Evaporation from drops, part i". *Chemical Engineering Progress*, **48**(3), pp. 141–146.
- [16] Ranz, W. E., and Marshall, W. R., 1952. "Evaporation from drops, part ii". *Chemical Engineering Progress*, **48**(4), pp. 173–180.
- [17] Wan, M. P., Chao, C. Y. H., Ng, Y. D., To, G. N. S., and Yu, W. C., 2007. "Dispersion of expiratory droplets in a general hospital ward with ceiling mixing type mechanical ventilation system". *Aerosol Science and Technology*, **41**(3), pp. 244–258.
- [18] Deevy, M., Sinai, Y., Everitt, P., Voigt, L., and Gobeau, N., 2008. "Modelling the effect of an occupant on displacement ventilation with computational fluid dynamics". *Energy and Buildings*, **40**(3), pp. 255–264.
- [19] Gao, N., and Niu, J., 2005. "Transient cfd simulation of the respiration process and inter-person exposure assessment". *Building and Environment*, **41**, pp. 1214–1222.
- [20] Qian, H., Li, Y., Nielsen, P. V., and Huang, X., 2009. "Spatial distribution of infection risk of sars transmission in a hospital ward". *Building and Environment*, **44**, pp. 1651–1658.
- [21] Qian, H., Li, Y., Nielsen, P. V., and Hyldgaard, C. E., 2008. "Dispersion of exhalation pollutants in a two-bed hospital ward with a downward ventilation system". *Building and Environment*, **43**(3), pp. 344–354.
- [22] Zhao, B., Zhang, Z., and Li, X., 2005. "Numerical study of the transport of droplets or particles generated by respiratory system indoors". *Building and Environment*, **40**(8), pp. 1032–1039.
- [23] Lai, A. C. K., and Cheng, Y. C., 2007. "Study of expiratory droplet dispersion and transport using a new eulerian modeling approach". *Atmospheric Environment*, **41**, pp. 7473–7484.
- [24] Tian, Z. F., Tu, J. Y., and Yeoh, G. H., 2007. "Cfd studies of indoor airflow and contaminant particle transportation". *Particulate Science and Technology*, **25**(6), pp. 555–570.
- [25] Derrick, D., Anderson, P., Gick, B., and Green, S., 2009. "Characteristics of air puffs produced in english "pa": Experiments and simulations". *Journal of the Acoustical Society of America*, **125**(4), pp. 2272–2281.
- [26] Graham, D. I., and James, P. W., 1996. "Turbulent dispersion of particles using eddy interaction models". *International Journal of Multiphase Flow*, **22**(1), pp. 157–175.
- [27] Seinfeld, J. H., 1986. *Atmospheric chemistry and physics of air pollution*. Wiley, New York.
- [28] Peyret, R., 1996. *Handbook of Computational Fluid Mechanics*. Academic Press Limited, USA.
- [29] Grigg, H. R., and Stewart, R. W., 1963. "Turbulent diffusion in stratified fluid". *Journal of Fluid Mechanics*, **15**, pp. 174–186.
- [30] Sangras, R., Kwon, O. C., and Faeth, G. M., 2002. "Self-preserving properties of unsteady round nonbuoyant turbulent starting jets and puffs in still fluids". *Journal of Heat Transfer*, **124**(3), pp. 460–469.
- [31] Kovaszny, L. S. G., Fujita, H., and Lee, R. L., 1974. "Unsteady turbulent puffs". *Advanced Geophysics*, **18B**, pp. 253–263.
- [32] Richards, J. M., 1965. "Puff motions in unstratified surroundings". *Journal of Fluid Mechanics*, **21**, pp. 97–106.
- [33] Morawska, L., 2006. "Droplet fate in indoor environments, or can we prevent the spread of infection?". *Indoor Air*, **16**, pp. 335–347.